JOC Article

Origins and Predictions of Stereoselective Antibody Catalysis: Theoretical Analysis of Diels−Alder Catalysis by 39A11 and Its Germ-Line Antibody

Xiyun Zhang, Qiaolin Deng, Sandy H. Yoo, and K. N. Houk*

Department of Chemistry and Biochemistry, University of California, Los Angeles, California 90095-1569

houk@chem.ucla.edu

Received June 10, 2002

The binding of enantiomeric haptens and transition states by the Schultz Diels−Alderase antibody 39A11 and its germ-line antibody were studied theoretically. The mechanisms by which one hapten and one transition state stereoisomer is recognized selectively are explored with docking simulations and quantum mechanical models. Transition states of the relevant Diels−Alder reaction were located with density functional theory. A prediction is made that the stereoselectivity of 39A11 will be achieved by two strategically placed hydrogen bonds and π-stacking interactions of the maleimide with a binding-site tryptophan, arranged so as to coordinate one enantiomeric transition state. Binding of other ligands by antibody 39A11 and the germ-line antibody has also been investigated. The polyspecific nature of 39A11 and its germ-line precursor was found to originate from the general ability of the binding pockets to achieve hydrophobic binding of small organic substrates. Comparison of the highly homologous progesterone and Diels−Alderase antibodies (DB3, 1E9, and 39A11) highlights the fact that differences of several key residues in the binding pockets are sufficient to confer selectivity for different antigens.

Introduction

Antibody catalysis[1−4] of several different types of Diels−Alder reactions[5] has been reported. Although absolute rate accelerations caused by these antibodies are modest, the control of stereochemistry is often excellent. For example, antibodies 13G5 and 22C8 accelerate the formation of one enantiomeric exo Diels−Alder adduct, while antibodies 7D4 and 4D5 selectively accelerate the formation of a single endo enantiomer.[6,7] The origins of this selectivity have been explored computationally.[8]

We now report a theoretical investigation of the Diels−Alderase antibody, 39A11, which catalyzes the addition of the acyclic diene **1** to the maleimide derivative **2** to give the cyclohexene product **3** (Scheme 1a).[9] Antibody 39A11 was produced from bicyclo[2.2.2]octene hapten **4**, a mimic of the boatlike transition state of the Diels−Alder reaction. The three-dimensional structures of the 39A11-hapten **4** complex and the germ-line precursor have been resolved at 2.4 and 2.1 Å resolution, respectively, by Romesberg et al.[10] The crystal structure of the 39A11-hapten **4** complex has provided a qualitative picture of how the antibody binds the hapten and how catalysis might be achieved. Several interesting questions remain. First, antibody 39A11 was raised against racemic hapten **4**, which involves two possible spatial arrangements of the −NHR and succinimide substituents attached to the bicyclooctene framework. In the X-ray crystal structure, only one kind of arrangement is observed, which we referred to as a hap1 a left-handed helical arrangement. While this is presumably a matter of chance, it is nonetheless interesting to understand how the stereodiscrimination occurs. Second, no direct evidence has been reported on the stereoselectivity of the antibody-catalyzed reaction. To address these first two questions, we explored how hapten stereoisomers and transition state stereoisomers bind in 39A11 theoretically. Our calculations predict the absolute stereoselectivity of the antibody-catalyzed reaction. Interactions leading to stereoselective binding of transition state stereoisomers have been modeled with quantum mechanical methods, which provide a more accurate way to quantitate the stereoselectivity of 39A11. Third, structural analysis indicates that affinity maturation of antibody 39A11 results in only two somatic mutations:

(1) Lerner, R. A.; Benkovic, S. J.; Schultz, P. G. *Science* **1991**, *252*, 659−667.
(2) Schultz, P. G.; Lerner, R. A. *Science* **1995**, *269*, 1835−1842.
(3) Wade, H.; Scanlan, T. S. *Annu. Rev. Biophys. Biomol. Struct.* **1997**, *26*, 461−493.
(4) Stevenson, J. D.; Thomas, N. R. *Nat. Prod. Rep.* **2000**, *17*, 535−577.
(5) Pindur, U.; Lutz, G.; Otto, C. *Chem. Rev.* **1993**, *93*, 741−761.
(6) Gouverneur, V. E.; Houk, K. N.; Pascual-Teresa, B.; Beno, B.; Janda, K. D.; Lerner, R. A. *Science* **1993**, *262*, 204−208.
(7) Yli-Kauhaluoma, J. T.; Ashley, J. A.; Lo, C.; Tucker, L.; Wolfe, M. M.; Janda, K. D. *J. Am. Chem. Soc.* **1995**, *117*, 7041−7047.
(8) Heine, A.; Stura, E. A.; Yli-Kauhaluoma, J. T.; Guo, C.; Deng, Q.; Beno, B.; Houk, K. N.; Janda, K. D.; Wilson I. A. *Science* **1998**, *279*, 1934−1940.
(9) Braisted A. C.; Schultz, P. G. *J. Am. Chem. Soc.* **1990**, *112*, 7430−7431.
(10) Romesberg, F. E.; Spiller, B.; Schultz, P. G.; Stevens, R. C. *Science* **1998**, *279*, 1929−1933.

10.1021/jo0203894 CCC: $22.00
Published on Web 11/19/2002

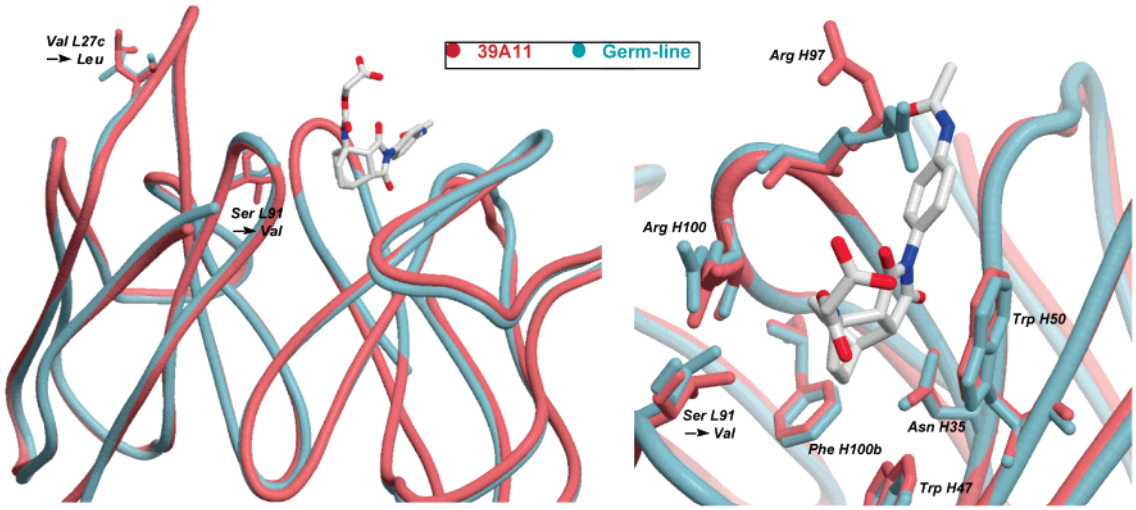

FIGURE 1. (Left) Ribbon superposition of the germ-line Fab without hapten and the mature 39A11-hapten **4** complex; (Right) a close-up view of the active site. (Re-created with permission from ref 10. Copyright 1998 American Association for the Advancement of Science.)

SCHEME 1. Diels−Alder Reactions Catalyzed by Antibodies 39A11 and 1E9 and the Hapten 9 for Another Homologous Antibody DB3

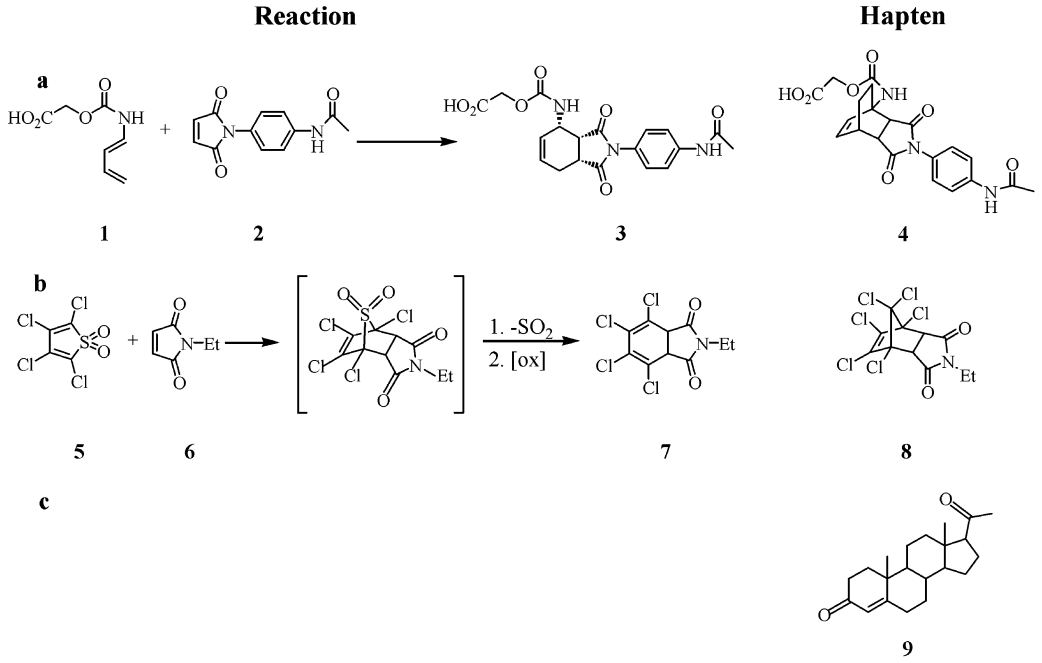

a Val → Leu substitution in CDRL1, which is distant from the active site, and a Ser → Val substitution in CDRL3, which has no direct contact with the hapten (Figure 1). To examine the evolution of this biological catalyst, we have also modeled the binding of hapten stereoisomers and transition state stereoisomers in the germ-line antibody. The stereoselectivities of germ-line and the germ-line catalyzed reaction are predicted and compared with those of mature antibody, 39A11. Fourth, the polyspecific nature of 39A11 and the germ-line antibody was inspected by modeling a variety of small organic molecules in their active sites. Finally, we have provided a genetic analysis that establishes the source of the different selectivities among the highly homologous antibodies, DB3, 1E9, and 39A11 (Scheme 1).

Background

The structure of the binding pocket of 39A11 and the germ-line with hapten **4** is shown in Figure 1.[10] The ligand is recognized by 89 van der Waals contacts with multiple aliphatic and aromatic residues. Notably, the succinimido group of the hapten π-stacks with the indole ring of Trp^{H50}. The polar and highly conserved residue Asn^{H35} in the binding pocket also donates a hydrogen bond to the succinimide carbonyl group of the hapten. The carbonyl oxygen of the carbamate moiety at the bridgehead position of hapten **4** appears to be orientated by a water-mediated hydrogen bond with Trp^{H50}. Schultz et al. proposed that catalysis by 39A11 involves both restriction of rotation and translation of the diene and

SCHEME 2. Structures of the Hapten Stereoisomers, Their Saturated Analogs and the Transition State Stereoisomers Complex

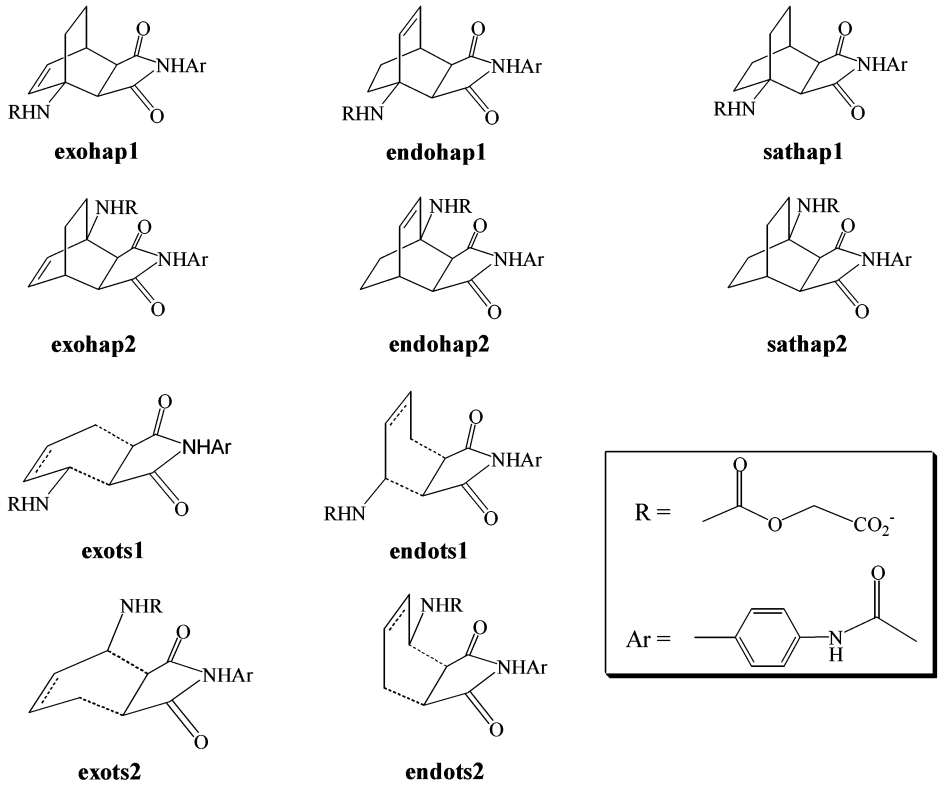

the dienophile, and hydrogen-bonding interactions that activate the maleimide toward the Diels−Alder reaction.[10]

Site-directed mutagenesis experiments were also reported.[11] Mutation of Asn^{H35} to Glu^{H35} in 39A11 results in a 5-fold decrease of catalytic activity. Arg^{H97} mutants of 39A11 (Arg^{H97}Gln, Arg^{H97}Ser, and Arg^{H97}Ala) also show decreased activities. It was proposed by Romesberg and Schultz that Arg^{H97} is involved in van der Waal interactions with the phenyl substituent of hapten **4**.[11] The crystal structure of the 39A11-hapten **4** complex reveals that the diene moiety is in contact with the CDRL3 region of 39A11 and is more loosely packed in the binding pocket compared to the dienophile moiety, which is in close contact with the CDRH3 region. Consequently, mutants with enhanced packing with the diene moiety, Val^{L91}Phe, Val^{L91}Tyr, and Pro^{L96}Phe, were generated and show increased catalytic activities from those of 39A11.

Antibody 39A11 has been found to be highly homologous to 1E9,[10,12,13] another Diels−Alder catalytic antibody raised against a hexachloronorbornene derivative (Scheme 1b), as well as to the progesterone-binding antibody DB3 (Scheme 1c).[10,14] Nevertheless, each of these three antibodies exhibits significant selectivity for a specific hapten. We have explored more fully the genetic analysis of these antibodies, with an eye to better understand the origins of selectivity and to determine how antibodies achieve different binding of substrate and transition state.

Computational Methods

Quantum mechanical calculations were carried out with the Gaussian 98 program.[15] Transition states were optimized with B3LYP/6-31G(d), which has been established as a good functional and basis set for calculating pericyclic reaction barriers.[16] Zero-point energy (ZPE) corrections were obtained from B3LYP/6-31G(d) frequency calculations and were scaled by 0.98. Single-point energies were evaluated with B3LYP/6-311++G(3d,3p). The CPCM model[17] was used to estimate the solvent (water) effect upon energetics.

All docking simulations were performed with the program AUTODOCK 3.0, which predicts the bound conformation of a flexible ligand in a rigid binding site.[18] The haptens were constructed and minimized using the AMBER force field in MACROMODEL 7.1.[19] The complete transition structures were obtained by adding substituents to the exo and endo

(11) Romesberg, F. E.; Schultz, P. G. *Bioorg. Med. Chem. Lett.* **1999**, *9*, 1741−1744.
(12) Xu, J.; Deng, Q.; Chen, J.; Houk, K.; Bartek, J.; Hilvert, D.; Wilson, I. *Science* **1998**, *286*, 2345−2348.
(13) Chen, J.; Deng, Q.; Wang, R.; Houk, K. N.; Hilvert, D. *ChemBioChem* **2000**, *1*, 255−261.
(14) Chen, J.; Wang, R.; Taussig, M.; Houk, K. N. *J. Org. Chem.* **2001**, *66*, 3021−3026.
(15) Frisch, M. J.; Trucks, G. W.; Schlegel, H. B.; Gill, P. M. W.; Johnson, B. G.; Robb, M. A.; Cheeseman, J. R.; Keith, T. A.; Petersson, G. A.; Montgomery, J. A.; Raghavachari, K.; Al-Laham, M. A.; Zakrzewski, V. G.; Ortiz, J. V.; Foresman, J. B.; Cioslowski, J.; Stefanov, B. B.; Nanayakkara, A.; Challacombe, M.; Peng, C. Y.; Ayala, P. Y.; Chen, W.; Wong, M. W.; Andres, J. A.; Replogle, E. S.; Gomperts, R.; Martin, R. L.; Fox, D. J.; Brinkley, J. S.; Defrees, D. J.; Bakwe, J.; Stewart, J. P.; Head-Gordon, M.; Gonzalez, C.; Pople, J. A. *Gaussian 98*; Gaussian Inc.: Pittsburgh, PA, 1998.
(16) Wiest, O.; Houk, K. N. *Topics in Current Chemistry* **1996**, *183*, 1; Wiest, O.; Montiel, D. C.; Houk, K. N. *J. Phys. Chem. A* **1997**, *101*, 8378.
(17) Barone, V.; Cossi, M. *J. Phys. Chem. A* **1998**, *102*, 1995−1999.
(18) Morris, G. M.; Goodsell, D. S.; Halliday, R. S.; Huey, R.; Hart, W. E.; Belew, R. K.; Olson, A. J. *J. Comput. Chem.* **1998**, *19*, 1639−1662.
(19) Mohamadi, F.; Richards, N. G. J.; Liskamp, W. C.; Lipton, M.; Canfield, C.; Chang, G.; Hendrickson, T.; Still, W. C. *J. Comput. Chem.* **1990**, *11*, 440−467.

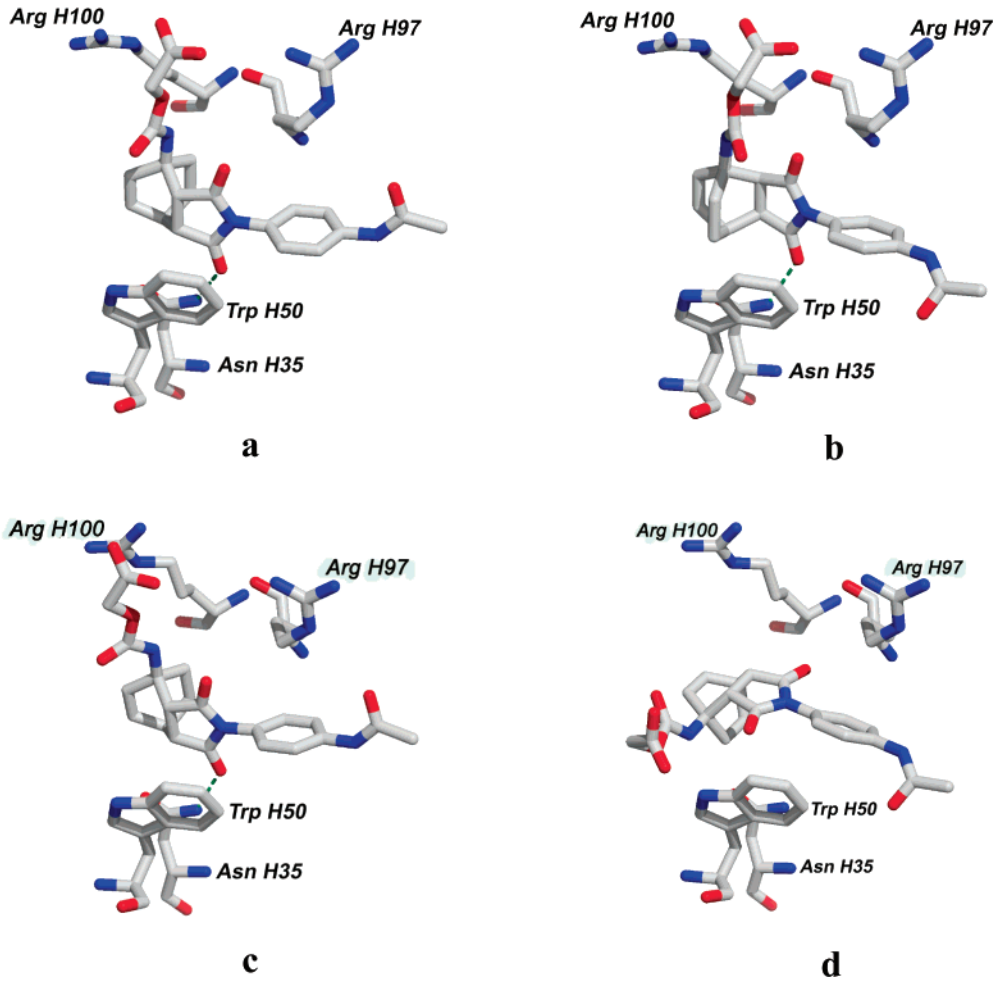

FIGURE 2. Haptens docked inside 39A11 and the germ-line antibody (a) hap1 inside 39A11; (b) hap2 inside 39A11; (c) hap1 inside the germ-line; (d) hap2 inside the germ-line.

quantum mechanical models located using B3LYP calculations. The substituents were then minimized using the AMBER force field. HF/6-31G(d) charges were assigned to atoms of all the structures for docking calculations. The X-ray crystal structures of 39A11 and the germ-line precursor were used in docking simulations after removing all the crystallographic water molecules. The genetic algorithm[18] was used in all the AUTODOCK calculations. One hundred simulations were performed for each system. Each simulation was composed of a maximum number of 250 000 energy evaluations and a maximum of 5 000 generations. All the rotatable torsions of the ligand molecules were allowed. All the other parameters relied on the default values provided by the AUTODOCK program. The lowest energy binding modes of ligand molecules were determined through the cluster analysis provided by AUTODOCK.

GRASP[20,21] was employed for the calculations of solvent accessible surface areas of haptens. GRASP, MOLSCRIPT,[22] and RASTER3D[23] were used to construct electrostatic potential surface images for the germ-line antibody, antibodies 39A11, 1E9, and DB3.

(20) Nicholls, A.; Sharp, K. A.; Honig, B. *Proteins: Struct. Funct. Genet.* **1991**, *11*, 281−296.

(21) The solvent accessible surfaces of all the haptens were constructed with the program GRASP[20] with a probe radius of 1.4 Å, and the area of each surface was then computed with functions implemented in GRASP.

(22) Kraulis, P. J. *J. Appl. Crystallogr.* **1991**, *24*, 946−950.

(23) Merrit, E. A.; Murphy, M. E. P. *Acta Crystallogr. Sect. D* **1994**, *50*, 869−873.

Results and Discussion

Docking of Four Hapten Stereoisomers and Their Saturated Analogues into 39A11 and the Germ-Line Precursor. Antibody 39A11 was elicited and then isolated by assay for binding to the chiral, but racemic hapten, **4**. The absolute configuration of the major product and the degree of stereoselectivity have not been determined. To probe the origins of stereoselective molecular recognition by antibodies, and to predict the absolute stereoselectivity of the catalysis, we have docked the two enantiomeric exo haptens (exohap1 and exohap2), the two enantiomeric endo haptens (endohap1 and endohap2), and their saturated analogues (sathap1 and sathap2) (Scheme 2) into the binding pockets of 39A11 and the germ-line antibody. Hap1 has the −NHR and succinimide substituents attached to the bicyclooctene framework so that the haptens are arranged in one stereochemical sense, a left-handed helical arrangement. Hap2 is the enantiomer of hap1 and the polar groups are now placed in a right-handed helical arrangement. The computations were designed to explore whether the hydrocarbon skeleton, particularly the position of the double bond, has any significance on binding, or whether the three-dimensional array of the hydrogen bonding groups alone determines to binding selectivity.

The preferred docking modes by the enantiomeric haptens are shown in Figure 2, parts a and b for 39A11

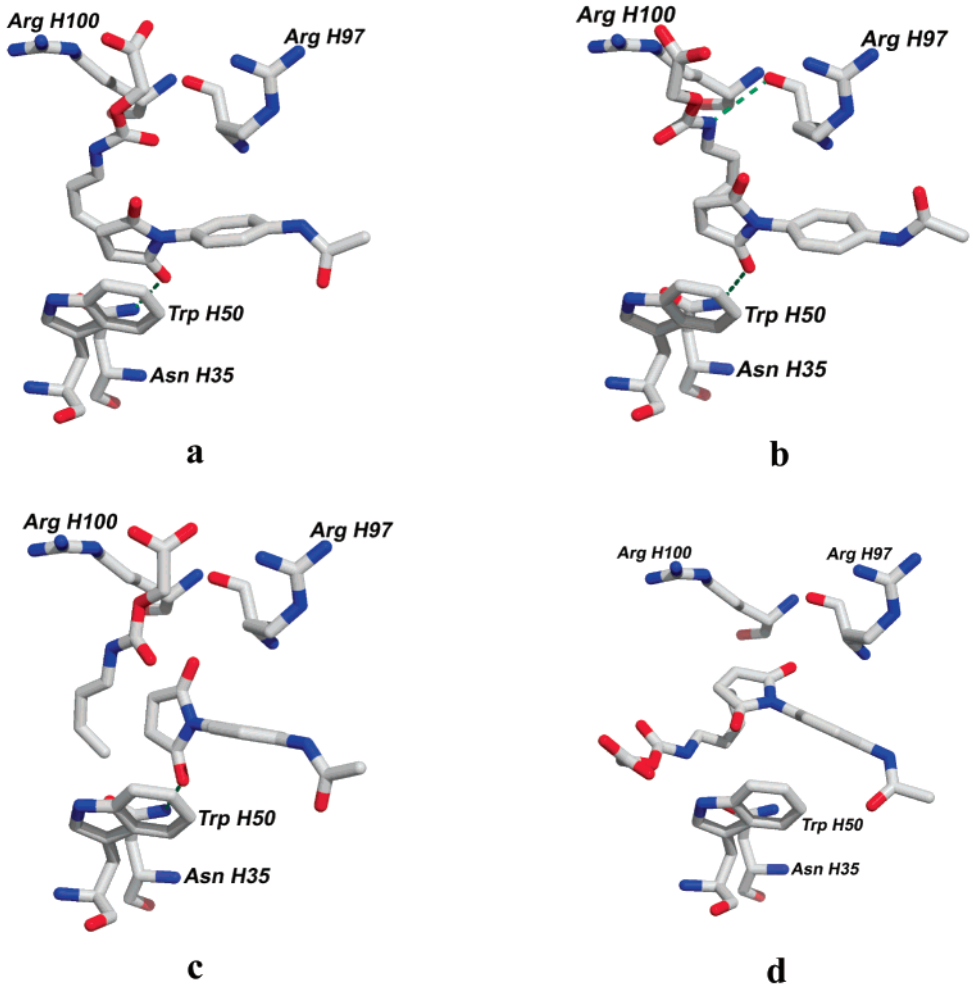

FIGURE 3. Transition states docked inside 39A11 (a) exots1; (b) endots1; (c) exots2; (d) endots2.

and parts c and d for the germ-line antibody. All of the structures of one configuration (exohap1, endohap1, and sathap1) have the same preferred binding mode inside 39A11, essentially identical to that shown in Figure 2a, while structures of the enantiomeric series (exohap2, endohap2, and sathap2) share the other binding mode, like that in Figure 2b. This is expected since the only difference among all the haptens in hap1 or hap2 is the position of the double bond, which plays no apparent role in binding. The hapten bound in the crystal structure (Figure 1) is essentially identical to the AUTODOCK prediction of the binding mode of the hap1 series. The key residues for 39A11-hap1 interactions include Asn^{H35}, which forms a hydrogen bond with the carbonyl group on the succinimido moiety, and Trp^{H50}, which provides π-stacking interactions with hap1. In the original crystal structure of the complex, the carboxylate group of the substituent interacts with Trp^{H50} through water-mediated hydrogen bonding. With the exclusion of water in the docking simulations, the carboxylate group has electrostatic interactions with Arg^{H97} and Arg^{H100} instead. The enantiomeric hap2 series does not have the same type of interactions. Asn^{H35} forms a hydrogen bond with the carbonyl oxygen of the succinimido moiety, but there are no π-stacking interactions between the succinimido ring and Trp^{H50}. Moreover, several different low-energy conformation clusters are observed for each molecule in the hap2 series, suggesting that the enantiomeric hapten does not bind to 39A11 in a specific way. Thus the binding pocket of 39A11 accommodates hap1 better than hap2, but both endo and exo hap1 can bind equally well.

In the germ-line antibody, different types of binding modes are also found for hap1 and hap2 (Figure 2, parts c and d). Except for the increased difference between the carboxylate substituent of the hapten and Arg^{H97}, the binding mode of hap1 in the germ-line (Figure 2c) is quite similar to that of hap1 in 39A11 (Figure 2a). The poor accommodation of hap2 by the germ-line antibody is more apparent (Figure 2d). Except for the electrostatic interactions between the substituent carboxylate group and Trp^{H50}, no hydrogen-bonding and π-stacking interactions are present. According to the docking calculations, the chiral discrimination occurs already in the germ-line precursor, and this eventually leads to the stereoselectivity of 39A11, which has a very similar binding pocket to the germ-line.

The fact that haptens within one series have essentially the same binding modes in 39A11 and the germ-line antibody suggests that the position or presence of a double bond is unimportant for binding. Second, the fact that haptens of series 1 are more favorable upon binding to both antibodies than haptens of series 2 suggests that the three-dimensional arrangement of the polar −NHR

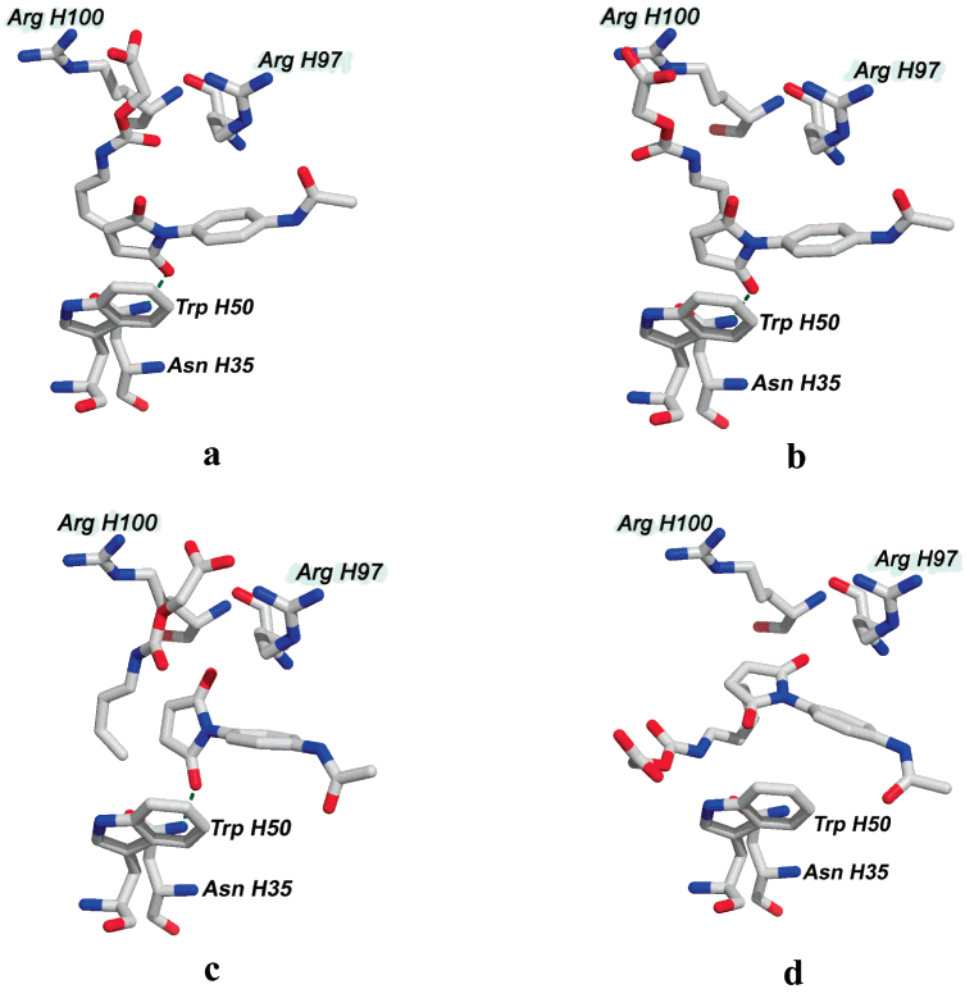

FIGURE 4. Transition states docked inside the germ-line (a) exots1; (b) endots1; (c) exots2; (d) endots2.

and succinimide substituents actually determines the magnitude of binding.

Docking of Four Stereoisomeric Transition States into 39A11 and the Germ-Line Precursor. The exo and endo transition states were computed with B3LYP quantum mechanical calculations (see later). Both enantiomers of the exo transition states (exots1 and exots2) and both enantiomers of the endo transition states (endots1 and endots2) have been docked into 39A11 and the germ-line antibody. The binding modes are shown in Figures 3 and 4, respectively. These docked structures are remarkably close to hapten structures. Both exots1 and endots1 dock inside 39A11 in a fashion that overlaps the docked hap1 very well (Figure 3, parts a and b). The hydrogen bond with the side chain of Asn^{H35} can make the dienophile component more electron-deficient, and consequently accelerate the Diels−Alder reaction. Moreover, the endots1 has an additional hydrogen bond between the amide group of its diene moiety and the backbone carbonyl oxygen of Arg^{H97}, which will make the diene moiety more electron-sufficient, and further accelerate the Diels−Alder reaction. The exots1 lacks this critical hydrogen bond. On the other hand, exots2 only hydrogen bonds with Asn^{H35}, and no electrostatic interactions between endots2 and the binding pocket of 39A11 are observed. Therefore, we predict that endots1 is stabilized best upon binding by 39A11.

The binding modes inside the germ-line antibody (Figure 4) are very similar to the corresponding ones inside 39A11 (Figure 3). Some variations that seem important involve endots1 in 39A11 (3b), where the backbone carbonyl oxygen of Arg^{H97} is 2.0 Å away from the amide hydrogen of endots1, close enough for a hydrogen bond in this arrangement. In the germ-line precursor (Figure 4b), the distance increases to 4.1 Å, and no hydrogen bond is formed between them. Thus the stereoselectivity of the mature antibody 39A11 is enhanced through better shape complementarity to endots1.

On the basis of the results of transition state docking, the three-dimensional arrangement of the polar −NHR and succinimide substituents, rather than the position of the double bond, determines the favorable transition state binding. This conclusion has a consequence for understanding the origins of stereoselectivity. The helicity observed in hap1 and ts1 types of structures seems more appropriate for the complementary helicity of the binding pockets, and this does not change during the maturation process from the germ-line precursor to antibody 39A11.

Theozyme Calculations. We explored whether the interactions identified from the docking experiments could account for stereoselective binding. Figure 5 summarizes the quantum mechanical model system studied; we call the arrangement of side chain functional groups

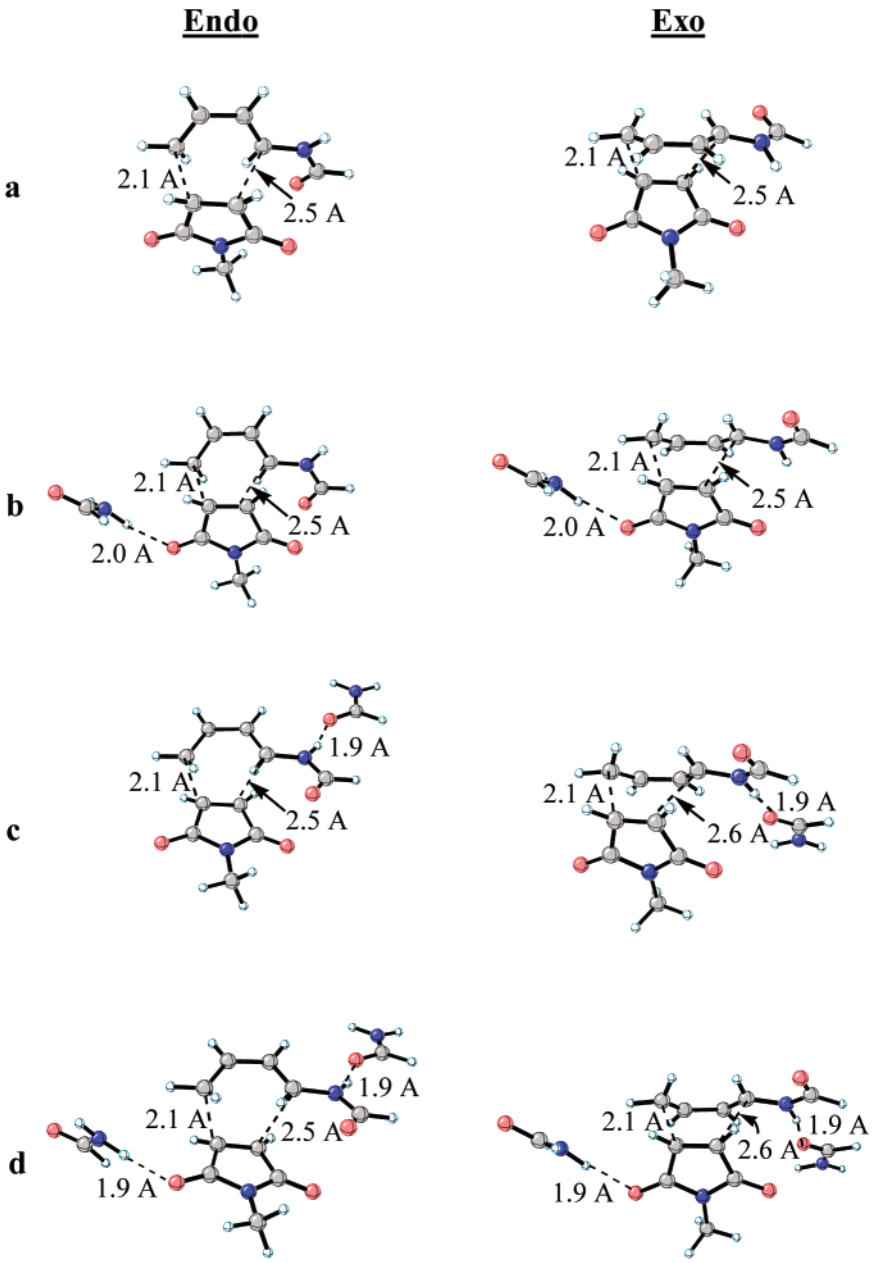

FIGURE 5. Transition structures from B3LYP/6-31G(d) optimizations: (a) without any hydrogen bonds; (b) with a hydrogen bond between dienophile and a formamide; (c) with a hydrogen bond between diene and a formamide; (d) with both hydrogen bonds.

around the transition states without the protein superstructure a "theozyme".[24] Endo and exo transition states of the reaction are shown in Figure 5a. Hydrogen bonding of the carbonyl oxygen of maleimide to a formamide molecule (Figure 5b) and hydrogen bonding of a formamide to the diene NH (Figure 5c) constitute model systems in which the two formamides correspond to the side chain amide group of Asn^{H35} and the backbone amide group of Arg^{H97}, respectively. Energetic results in the gas phase are summarized in Scheme 3. The differences in the starting energies are due to substrate stabilization by the hydrogen bonds.

In the gas phase, the activation energy for the endo pathway is 5.2 kcal/mol lower than that of the exo pathway (Scheme 3a). Favorable secondary orbital interactions and electrostatic interactions in the endo transition state are responsible for this preference. The energy difference decreases to 3.4 kcal/mol in water. The calculated preference for the endo adduct is in accord with the formation of endo product observed in solution.[9]

When one formamide molecule was added to simulate the hydrogen bond between the carbonyl oxygen on the dienophile and the side chain amide of Asn^{H35}, the hydrogen bond decreases the activation energy of the endo transition structure by 1.2 kcal/mol, which lowers the activation barrier of the exo transition structure by 1.4 kcal/mol. The endo transition state is still favored by

(24) Tantillo, D. J.; Chen, J.; Houk, K. N. *Curr. Opin. Chem. Biol.* **1998**, *2*, 743−750.

SCHEME 3. Energy Diagram for Uncatalyzed and Catalyzed Diels–Alder Reactions. (Energies are in kcal/mol at B3LYP/6-311++G(3d,3p)//B3LYP/6-31G (d))[a]

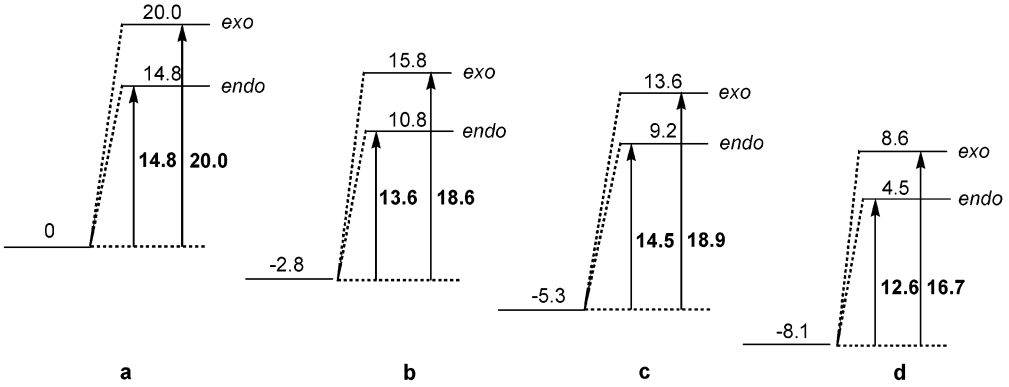

[a] Key: (a) without any hydrogen bond; (b) with a hydrogen bond between dienophile and a formamide; (c) with a hydrogen bond between diene and a formamide; (d) with hydrogen bonds. Activation barriers are shown in bold.

CHART 1. Sructures of Hapten 4 and Ligands A through I Reported by Schultz for the Cross-Link Experiments of 39A11 and Its Germ-Line Precursor[a]

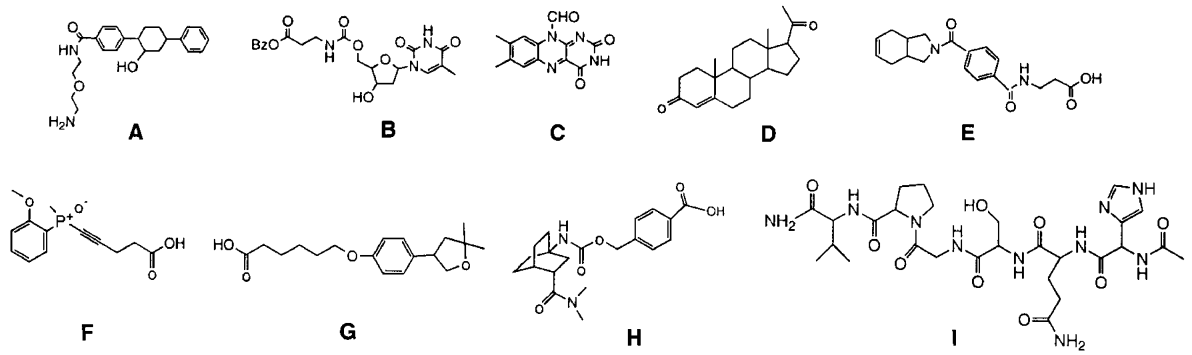

[a] Reprinted with permission from ref 10. Copyright 1998 American Association for the Advancement of Science.

5.0 kcal/mol (Scheme 3b). When another formamide molecule was employed to simulate the hydrogen bond between the NH group on diene and the backbone amide oxygen of Arg^{H97}, the activation barriers for the endo and exo pathway are lowered by 0.3 and 1.1 kcal/mol, respectively (Scheme 3c). The endo transition state is favored by 4.4 kcal/mol. It is found that with the presence of both hydrogen bonds, the effects are additive. The activation barriers for the endo and exo pathways are decreased by 2.2 and 3.3 kcal/mol, respectively. The endo pathway is still favored by 4.1 kcal/mol (Scheme 3d). These estimates are for the gas phase and should be reduced in solution or the antibody interior.

The docking results indicate that 39A11 and the germ-line bind exots1 and endots1 more strongly than either ts2. All the hydrogen bonding and π-stacking interactions determined between each pair of exots1/endots1 and 39A11/germ-line are listed in Table 1. In 39A11, the endots1 is bound better because the exots1 does not allow the favorable hydrogen bonding with Arg^{H97}, while the germ-line binds endots1 and exots1 equally well. Both endots1 and exots1 have π-stacking interactions. Hydrogen bonding differences alter binding of endo and exo transition states. Therefore, by comparing the activation energies for theozymes d-endo and b-exo (Scheme 3), it is predicted that in the 39A11-catalyzed reaction, E_a^{endo} is 12.6 kcal/mol, E_a^{exo} is 18.6 kcal/mol, and the preference for the endo is about 6.0 kcal/mol (Table 2). Similarly, in the germ-line catalyzed reaction, E_a^{endo} is 13.6 kcal/mol, E_a^{exo} is 18.6 kcal/mol, and the preference for the endo is 5.0 kcal/mol. The endo preference is enhanced in both the germ-line and 39A11 relative to water. It is predicted that a (3*S*,4*R*,5*R*) product will be obtained as the major product from both antibody catalysts.

TABLE 1. Comparison of Nonbonded Interactions Located by Docking Experiments and the Corresponding Quantum Mechanical Theozymes

		Trp^{H50}	Asn^{H35}	Arg^{H97}	theozyme
uncatalyzed	exots1				a-exo
	endots1				a-endo
39A11	exots1	π-stacking	H-bonding		b-exo
	endots1	π-stacking	H-bonding	H-bonding	d-endo
germ-line	exots1	π-stacking	H-bonding		b-exo
	endots1	π-stacking	H-bonding		b-endo

TABLE 2. Comparison of Activation Barriers Computed for Uncatalyzed and Antibody-Catalyzed Diels–Alder Reactions Using Models Described in the Text

	E_a^{exots1} (kcal/mol)	$E_a^{endots1}$ (kcal/mol)	$E_a^{exots1} - E_a^{endoeo1}$ (kcal/mol)
uncatalyzed[a]	20.0	14.8	5.2
uncatalyzed[b]	16.5	13.1	3.4
39A11	18.6	12.6	6.0
germ-line	18.6	13.6	5.0

[a] In the gas phase. [b] In water.

TABLE 3. Dissociation Constants, Binding Free Energies, Calculated BSA of Hapten 4 and Ligands A through I with Antibodies 39A11 and the Germ-Line

		4	A	B	C	D	E	F	G	H	I
39A11	K_d[a] (μM)	0.01	5.02	4.9	8.4	0.40	5	20	10	10	0.11
	ΔG_{exp}[b] (kcal/mol)	−11	−8	−7	−7	−9	−7	−6	−7	−7	−10
	ΔG_{cal} (kcal/mol)	−11	−12	−13	−9	−10	−10	−9	−12	−10	−13
	BSA (Å^2)	371	392	428	288	301	334	302	366	376	566
germ-line	K_d[a] (μM)	0.38	3.10	2.4	7.9	0.40	5	20	10	10	0.10
	ΔG_{exp}[b] (kcal/mol)	−9	−8	−8	−7	−9	−7	−6	−7	−7	−10
	ΔG_{cal} (kcal/mol)	−11	−11	−13	−9	−10	−11	−10	−12	−11	−14
	BSA (Å^2)	412	410	412	270	308	376	278	348	384	554

[a] Experimental K_d values are reported by Schultz et al.[10] [b] ΔG_{exp} values are calculated from K_d.

TABLE 4. Comparison of the Sequences for Antibodies 39A11, DB3, 1E9, and Their Germ-Line Antibodies[a]

	CDRL1		
Vκ1A	DVVMTQTPLSLPVSLGDQASISC	RSSQSLVHSNGNTYLH	WYLQKPGQSPKLLIY
39A11	----------	----------L----------	----------
DB3	----------I----------N----------	--- --------I----------	----------
1E9	EL----------	----------	----------

	CDRL2		CDRL3	
Vκ1A	KVSNRFS	GVPDRFSGSGSGTDFTLKISRVEAEDLGVYFC	SQSTHVP	
39A11	----------	----------	---V--------	PTFGGGTKLEIK
DB3	----------Y	----------I-------	-----S-------	----------
1E9	----------	----------G----------I----------	F--- ----FF	----------

	CDRH1		CDRH2	
VSM9	QIQLVQSGPELKKPGETVKISCKASGYTFT	NYGMN	WVKQAPGKGLKWMG	WINTYTGEPTYADDFKG
39A11	----------	----------	----------	----------
DB3	----------A---	-------V--	--------E--------E----------	------I----------V----------
VFM11	----------	----------	----------	----------
1E9	----------M--	----------	----------	----------

	CDRH3		
VSM9	RFAFSLETSASTAYLQINNLKNEDTATYFCAR		
39A11	----------VQ	AERLRRTFDY	WGAGTTVTVSS
DB3	----------E----------TR	GDYVNWYFDV	----------
VFM11	----------M----------		
1E9	----------M----------AR	GTTIVRAMDY	-----Q-----SL------

[a] Abbreviations for the amino acid residues are as follows: A, Ala; C, Cys; D, Asp; E, Glu; F, Phe; G, Gly; H, His; I, Ile; K, Lys; L, Leu; M, Met; N, Asn; P, Pro; Q, Gln; R, Arg; S, Ser; T, Thr; V, Val; W, Trp; and Y,Tyr. Dashes represent identical residues. The amino acid sequences are numbered according to the Kabat numbering.

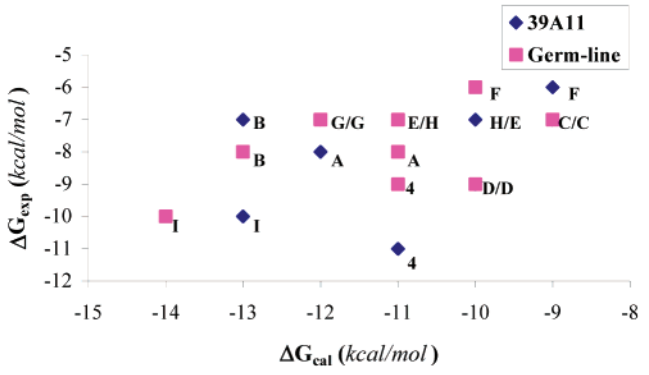

FIGURE 6. Plot of ΔG_{exp} and ΔG_{cal}.

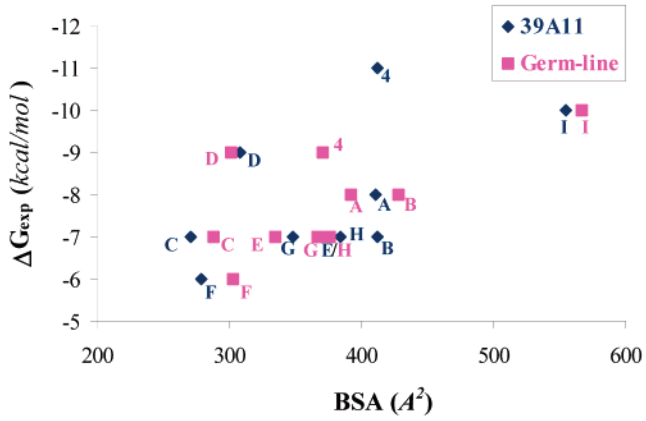

FIGURE 7. Plot of ΔG_{exp} and BSA.

Docking of Ligands A through I into 39A11 and the Germ-Line Precursor. Binding experiments show that the binding pockets of 39A11 and the germ-line are polyspecific.[10] We explored the docking of ligands **A** through **I** (Chart 1) in the binding pockets of 39A11 and the germ-line precursor to determine the origins of polyspecificity.

The AUTODOCK free energies of binding for the docked structures with the greatest binding free energy are listed in Table 3. The scoring function gives uncertainty of ΔG_{cal} of ±2 kcal/mol,[18] so all of the binding free energies are nearly the same (from − 9 to −14 kcal/mol) within computational error. The calculations predict binding of about 0.1 nM to 1 μM, whereas the experiment values range from 0.01 to 20 μM. The polyspecificity of

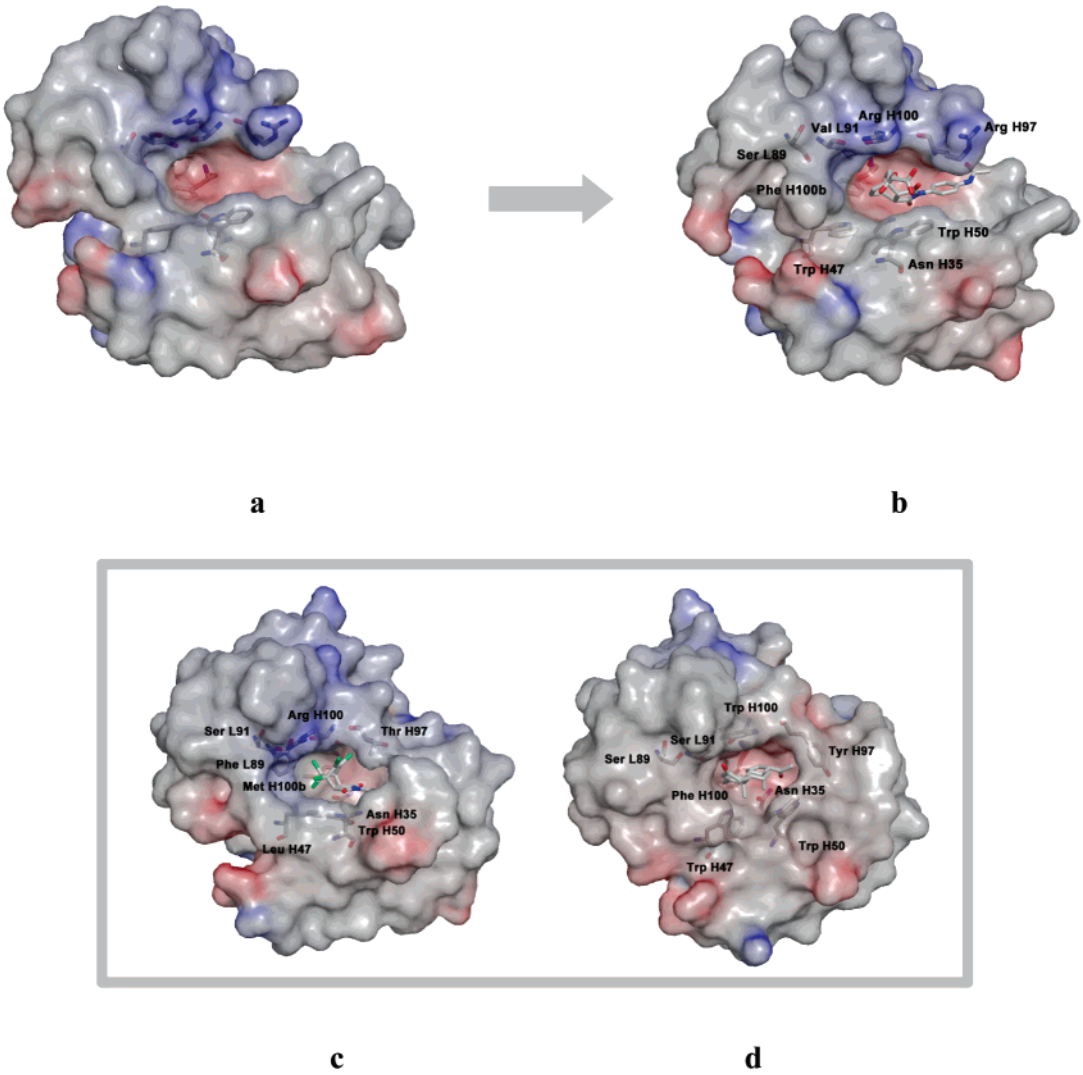

FIGURE 8. Binding pockets of germ-line (a), 39A11-hapten **4** complex (b), 1E9-hapten **8** complex (c), and DB3-hapten **9** complex (d) as determined by X-ray structure analysis. Electrostatic potential surfaces were constructed using residues within 16 Å of the hapten. Blue and red are positive and negative potentials, respectively.

TABLE 5. Comparison of the Important Binding Cavity Residues for Antibodies 39A11, DB3, and 1E9[a]

	CDRH1	Framework	CDRH2	CDRH3			CDRL3	
39A11	Asn^{H35}	Trp^{H47}	Trp^{H50}	Arg^{H97}	Arg^{H100}	Phe^{H100b}	Ser^{L89}	Val^{L91}
DB3	Asn^{H35}	Trp^{H47}	Trp^{H50}	Tyr^{H97}	Trp^{H100}	Phe^{H100b}	Ser^{L89}	Ser^{L91}
1E9	Asn^{H35}	Leu^{H47}	Trp^{H50}	Thr^{H97}	Arg^{H100}	Met^{H100b}	Phe^{L89}	Ser^{L91}

[a] All the residues are numbered according to Kabat numbering.

39A11 and the germ-line has been determined experimentally by the measurement of dissociation constants (K_d) (Table 3).[10] The relationship between ΔG_{exp} and ΔG_{cal} is shown in Figure 6. There is only a rough relationship between the computed binding free energy change and the binding affinity found experimentally.

The buried surface area upon binding (BSA) has been found to correlate with binding for a variety of hosts in aqueous solution. The buried surface area values were calculated for the hapten **4** and each of the ligands (Table 3). The relationship between ΔG_{exp} and BSA is shown in Figure 7. There is considerable scatter here also, but ligand **I** has the biggest BSA and the smallest dissociation constant in the germ-line. For 39A11, the hapten **4** deviates significantly, and it binds even tighter to 39A11 than ligand **I**. This suggests that maturation maintains hydrophobic binding, as reflected in the BSA, but maturation from the germ-line to 39A11 significantly increases the specific interactions between the ligand and the protein.

Genetic and Sequence Analysis of 39A11, 1E9, and DB3. As we mentioned before, catalytic antibody 39A11 is highly homologous with antibodies 1E9 and DB3. All three antibodies have the same sequence length and similar hydrophobic binding pockets, but they have quite different specificities and characteristics. Schultz et al. previously analyzed the genetic origins of these antibodies,[10] but we have elaborated this analysis below.

For 39A11, DB3, and 1E9, the light chain variable regions that include the hypervariable complementarity determining regions, CDRL1, CDRL2, and CDRL3, are all encoded by the V_κ1A gene, which is a part of the V_κ1 gene family (Table 4).[25] In contrast, the heavy chain variable regions, including CDRH1 and CDRH2, of 39A11 and DB3 utilize gene VSM9, while those of 1E9 utilize gene VFM11.[26] VSM9 and VFM11 both belong to the VGAM3.8 gene family with only one nucleotide base difference that encodes Thr^{H87} in VSM9 and Met^{H87} in VFM11. This difference occurs in the framework region of antibodies and has no significant role in antigen binding. On the basis of these similarities, 39A11, DB3, and 1E9 are highly homologous antibodies.

However, much variability is observed in the CDRH3 region. Generally, among the six CDRs (CDRH1−3 and CDRL1−3), CDRH3 is in the closest contact with hapten, and it contributes many of the residues in the binding pocket. The key residue mutations in the binding pocket of an antibody can be considered as hapten and immunization determined rather than germ-line encoded, since these variations determine the selectivity for different haptens. Most of the variations of these antibodies are determined by two genes, the variable (V) gene and the joining (J) gene. The shape of the hydrophobic binding pocket is the result of these genes. CDRH3, however, is encoded by the joining gene and diversity (D) gene, as well as random nucleotides added by the enzyme terminal deoxynucleotidyl transferase and not by the V_H gene. We have attempted to assign the most likely D_H and J_H genes for each antibody but this proves to be very difficult since the overlap between the antibody amino acid sequence of this region and the coding frames in all the D and J gene families available is found to be extremely poor.

The differentiation of a few key residues, especially those located in the CDRH3 region of otherwise highly homologous antibodies, determines the distinct characteristics of these antibodies. This can be visualized from the protein surface images in Figure 8. The surfaces were constructed using the residues within 16 Å of the haptens and were mapped with electrostatic potentials, where blue represents positive potentials (low electron density) while red represents negative potentials (high electron density). As shown in Figure 8b, the binding pocket of antibody 39A11 is rather polar and open, which is very similar to the binding pocket of its germ-line precursor (Figure 8a). The catalytic ability of 39A11 mainly comes from the favorable electrostatic interactions that stabilize the transition states more than the reactants. As discussed before, the critical hydrogen bond with Arg^{H97} is only observed in the binding of endots1 to mature antibody 39A11. However, the binding pocket is a relatively shallow and open cavity, which explains the polyspecific nature of 39A11.

Comparison of the binding pockets between 39A11 and DB3 shows differences in three key residues (Table 5). Arg^{H97}, Arg^{H100}, and Val^{L91} in 39A11 are changed to Tyr^{H97}, Trp^{H100}, and Ser^{L91} in DB3, respectively. The first two residue differences make the binding pocket of DB3 much less polar, which is better for hydrophobic binding. It is also notable that the binding cavity of DB3 becomes closed and consequently exhibits better shape complementary to the hapten.

Comparison of the binding pockets of 39A11 and 1E9 shows differences in five key residues. Trp^{H47}, Phe^{H100b}, and Ser^{L89}, which are conserved in 39A11 and DB3, are changed to Leu^{H47}, Met^{H100b}, and Phe^{L89} in 1E9, respectively. In addition, there are two $Arg^{H97} \rightarrow Thr^{H97}$ and $Val^{L91} \rightarrow Ser^{L91}$ changes from 39A11 to 1E9 that also differ between 39A11 and DB3. The five key residue changes observed further improve the binding pocket of 1E9, which is shown to be the most efficient Diels−Alderase antibody documented to date.[12]

Conclusion

Antibody 39A11 and its germ-line precursor can accommodate all four stereoisomeric haptens and their saturated analogues, preferring one left-handed helical arrangement (hap1 type) of the polar functionalities on the haptens. Endo and exo transition structures with the same arrangement of functional groups fit into the binding pockets better than the other type of transition structures. Both docked exots1 and endots1 can have π-stacking interactions with Trp^{H50} and hydrogen bonding with Asn^{H35} in 39A11. Therefore they are more stabilized than exots2 and endots2. The endots1 is inherently more favored than exo, and it fits into the pocket with one more hydrogen bond with Arg^{H97} than exots1. We predict that the 39A11-catalyzed reaction should further accelerate the formation of an endo product, with stereochemistry, (3*S*,4*R*,5*R*), corresponding to endots1. The chiral discrimination appears even in the germ-line antibody, where exots1 and endots1 are the most favored configurations. In the germ-line precursor, the Arg^{H97} residue is farther away from the transition state and no hydrogen bond is found between Arg^{H97} and endots1. This difference indicates that shape complementarity from the immature germ-line antibody to mature 39A11 increases the stereoselectivity of the antibody.

Acknowledgment. We are grateful to the National Science Foundation and National Institute of General Medical Sciences, National Institutes of Health for financial support of this research and to the National Center for Supercomputing Applications, University of Illinois at Urbana−Champaign and the UCLA Office of Academic Computing for computational resources. We thank Professor Raymond Stevens for X-ray coordinates and helpful discussions.

Supporting Information Available: Cartesian coordinates and total computed energies for theozymes. This material is available free of charge via the Internet at http://pubs.acs.org.

JO0203894

(25) Goldsby, R. A.; Kindt, T. J.; Osborne, B. A.; Kuby, J. *Immunology*; W. H. Freeman & Co.: San Francisco, 2000.

(26) Sims, M. J.; Krawinkel, U.; Taussig, M. J. *J. Immunol.* **1992**, *149*, 1642−1645.